CrystEngComm

Accepted Manuscript

ROYAL SOCIETY OF CHEMISTRY

www.rsc.org/crystengcomm

Cite this: DOI: 10.1039/c0xx00000x

www.rsc.org/xxxxxx

ARTICLE TYPE

Facile synthesis of hierarchical hollow MoS_2 nanotubes as anode material for high-performance lithium-ion batteries

Guangda Li,[a] Xiaoying Zeng,[b] Tiandong Zhang,[b] Wanyong Ma,[a] Wenpeng Li,[a] and Meng Wang*[b]

Received (in XXX, XXX) Xth XXXXXXXXX 20XX, Accepted Xth XXXXXXXXX 20XX

DOI: 10.1039/b000000x

Hierarchical hollow MoS_2 nanotubes were successfully synthesized using $Na_2MoO_4·2H_2O$, $MnCl_2·4H_2O$ and $(NH_4)_2CS$ through simple solvothermal reaction. The formation of hierarchical hollow MoS_2 nanotubes was based on the intermediate $MnMoO_4$ as a self-sacrificed template. The hollow MoS_2 nanotubes exhibited improved reversibility and cycling performance compared with the solid MoS_2 when evaluated as an anode material for lithium-ion batteries. A high capacity of 727 mAh g^{-1} could be retained after 100 cycles at a current density of 100 mA g^{-1}. The rate capability of the hollow MoS_2 nanotubes also improved. The hierarchical hollow MoS_2 nanotubes could be still maintained at 480 mAh g^{-1} at a current density of 1000 mA g^{-1}. The enhanced lithium ion storage performance of the hierarchical hollow MoS_2 nanotubes in terms of reversible capacity, cycling performance, and rate capability can be attributed to their hierarchical surface and hollow tube structure.

1. Introduction

Lithium ion batteries (LIBs) have become an important power source because of their high energy density and high voltage. Graphite is extensively used as commercial anode material for LIBs because of its low cost, good conductivity, and structural stability during cycling.[1-3] However, graphite materials have relatively low theoretical capacity (372 mAh g^{-1}), and could not meet the demand for high-power tools and electric vehicles. Therefore, considerable efforts have been devoted to find high capacity and stable performance anode materials to replace graphite anodes.[4-6]

Recently, layered transition metal sulfides, such as MoS_2, WS_2, ZrS_2, and SnS_2, have gained considerable interest as candidates for anode materials because of their high theoretical capacities and unique layered structure.[7-9] As a typical layered metal sulfide, MoS_2 has similar structure to graphite. In layered MoS_2, the Mo and S atoms are interconnected by strong covalent forces to form two-dimensional layers, which are then further stacked by weak van der waals interaction. The layered structure enables facile insertion and extraction of Li^+ ions without a significant change in volume. MoS_2 has attracted significantly attention for LIBs because of its 4-electron transfer reaction during the cycles which can achieve a much higher specific capacity in theory (＞670 mAh g^{-1}).[9] The interlayer space can provide excellent environment to accommodate Li ions.[10] This special structure features determine MoS_2 may become a kind of excellent anode material in the future.

Various nanostructured MoS_2 materials, such as nanospheres,[11] nanotubes,[12] nanosheets,[13] and nanorods[14] have been reported as anode materials for LIBs. Although some of these materials have shown relatively high capacities, unsatisfactory cycling stability and rate capability obstructed their application as anode materials for LIBs. Considerable efforts have been devoted to improve the cycling and rate performance of MoS_2 electrode. One of the most widespread methods is to construct composite materials using MoS_2 and carbonaceous materials.[15-21] For example, Wang prepared MoS_2/single-walled carbon nanotubes to form novel composite thin films for lithium battery applications. The capacity of these composite materials is approximately 992 mAh g^{-1} after 100 cycles.[22] Zhou developed a facile strategy to fabricate MoS_2 impregnated CMK-3 nanocomposite. The MoS_2@CMK-3 nanocomposite showed an improved cycling stability of 602 mAh g^{-1} at 250 mA g^{-1} within 100 cycles.[23] Given the discovery of graphene, the synthesis of MoS_2/graphene composite materials for LIBs has attracted a great deal interests.[24-27] In the literature, single-layer MoS_2/graphene exhibited the largest reversible capacity (1116 mAh g^{-1}) with negligible fading capacity, retaining a high specific capacity of 850 mAh g^{-1} after 250 cycles.[28] MoS_2 nanoflakes/grapheme have been fabricated and exhibited very good electrochemical performance at high current densities. Even at 8000 mA g^{-1}, the discharge capacity is as much as 516 mAh g^{-1}.[29] The cycling stability and rate capability are improved significantly by the hybrid carbon approach. However, the preparation process of these composite materials tends to be more complex. To date, preparing MoS_2 anode materials through a simple method is still a challenging task in developing high-performance LIBs.

It is well known that a design effective nanostructure is a very important means to improving electrochemical performance such as hierarchical architecture.[30,31] Hierarchical hollow structure means that the active sites for Li^+ ions storage are significantly increased. In addition, it becomes much easier for electrolyte and Li^+ ions to enter and react with inside active materials, and

resulting in a high specific capacity. The large surface area of the hierarchical structure could facilitate storage of more Li^+ ions, and the hollow tube can buffer the volume change during the discharge/charge cycles, thus leading to enhanced cycling performance. For example, Xu constructed a type of ultrathin MoS_2 nanosheet on CMK-3 hybrid nanostructure by a hydrothermal process. The MoS_2@CMK-3 composite electrode exhibited a large capacity of 934 mAh g^{-1} even after 150 cycles at 400 mA g^{-1}. Authors think that hierarchical architecture of MoS_2 nanosheets makes a prominent contribution to the excellent electrochemical performance.[32]

In the present work, a facile process for the synthesis of hollow hierarchical one-dimensional (1D) MoS_2 nanotubes is introduced using $Na_2MoO_4{\cdot}2H_2O$, $MnCl_2{\cdot}4H_2O$, and $(NH_2)_2CS$ as starting materials at 210 ℃ for 16 h. Electrochemical tests indicated that the synthesized MoS_2 hollow nanotubes exhibited higher capacity and better cycling stability as anode materials for LIBs. The first discharge and charge capacities were 1197 and 896 mAh g^{-1}, showing an efficiency of 87%. The capacity was still retained at 727 mAh g^{-1} after 100 cycles at current density of 100 mA g^{-1}. The causes of performance improvement were also analyzed. The hollow cavity and hierarchical architecture can increase the interface contact area between electrode and electrolyte and supply space for volume change during the discharge-charge processes. Furthermore, the hierarchical architecture can provide fast transport channels for lithium ions and the thin walls can great reduce lithium ion diffusion path.

2. Experimental

2.1 Sample preparation

In a typical procedure, 1.165 g $Na_2MoO_4{\cdot}2H_2O$, 0.312 g $MnCl_2{\cdot}4H_2O$ and 1.37 g $(NH_2)_2CS$ were dissolved in 30 ml deionized water and 10 ml absolute ethanol. After stirring for 30 min, the solution was transferred into a 50 ml Teflon-lined stainless steel autoclave and sealed tightly, heated at 210 ^oC for 16 h. After cooling naturally, the black precipitates were collected and washed with diluted hydrochloric acid and deionized water several times, and dried at 60 ^oC for 5 h in a vacuum oven. Finally, the hierarchical hollow MoS_2 nanotubes can be obtained. MoS_2 nanoflowers can be obtained when the reagents dissolved in 30 ml absolute ethanol and 10 ml deionized water, and other reaction conditions have no changed.

2.2 Characterization

The X-ray powder diffraction (XRD) patterns were performed on a Bruker D8 advanced X-ray diffractometer equipped with graphite monochromatized Cu Kα radiation (λ=1.5418 Å). The morphologies of the samples were observed through scanning electron microscopy (SEM) and transmission electron microscope (TEM) measurements, which were carried out on a JSM-7600F field emission instrument and a Hitachi H-7000 TEM, respectively. High-resolution transmission electron microscope (HRTEM) images were carried out on a JEOL 2010 Transmission electron microscope with an accelerating voltage of 200 KV. N_2 adsorption/desorption isotherms are measured at 77 K on a Micromeritics ASAP 2020 volumetric adsorption system.

2.3 Electrochemical measurements

The electrochemical tests were performed under ambient temperature using two-electrode coin cell (size: 2032) with lithium serving as both the counter electrode and the reference electrode. The working electrodes was prepared by mixing 70 wt% active materials (MoS_2), 10 wt% carboxymethy-lcellulose sodium (CMC), and 20 wt% acetylene black onto a copper foil substrate. The electrodes were dried at 80 ℃ in a vacuum oven for 24 h. Celgard 2300 microporous polypropylene membrane was used as separator. The electrolyte consisted of a solution of 1 M $LiPF_6$ in an ethylene carbonate/dimethyl carbonate/diethyl carbonate (EC/DMC/DEC, 1:1:1, volume ratio). The cell assembly was carried out in an argon-filled glovebox with both the moisture and the oxygen conten below 1 ppm. The discharge/charge tests of the samples were performed on a Land battery test system (CT2001A). The cyclic voltammetry (CV) test was carried out in the potential window of 0.01 V to 3.0 V by an electrochemical workstation (CHI 760C). The electrochemical impedance spectroscopy (EIS) was measured on an FRA-520 (MaterialsMates, Italia) connected to a Potentiostat-510 (MaterialsMates) in the frequency range from 100 KHz to 0.01 Hz.

3. Results and discussion

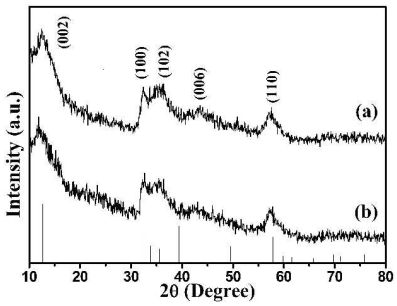

Fig. 1 XRD patterns of the (a) MoS_2 hollow nanotubes and (b) MoS_2 nanoflowers.

Fig. 1 shows the XRD patterns of the hollow MoS_2 nanotubes and MoS_2 nanoflowers synthesized by the hydrothermal method. Both as-prepared MoS_2 have the same phase and chemical composition. All diffraction peaks of the MoS_2 were in good agreement with the standard hexagonal structure (JPCDS no. 37-1492). Fig. 1 shows that the strong (002) diffraction peak appeared at 14.2^o with a d-spacing of 0.62 nm, indicating a well-formed layered structure during the growth using the proposed synthesis method.

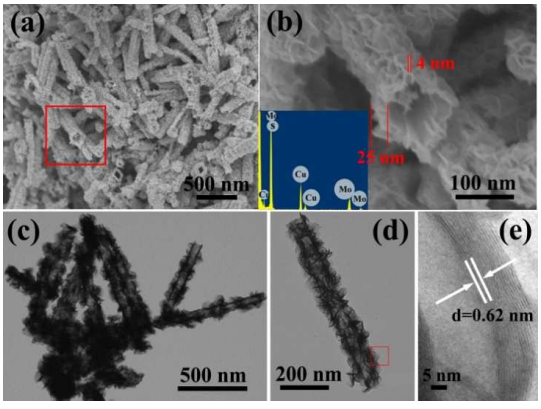

Fig. 2 (a) SEM image of the hollow MoS_2 nanotubes, (b) magnified SEM and EDS image (inset), (c) and (d) TEM images of the hollow MoS_2 nanotubes, (e) HRTEM image of the MoS_2 nanosheet.

Fig. 2 shows the morphologies of the hollow MoS_2 nanotubes. The nanotubes were approximately 100 nm in diameter and 500-1000 nm in length, as comfirmed by SEM image in Fig. 2a. Open ends can be observed from hollow MoS_2 nanotubes. The nanotubes are composed of ultrathin nanosheets. Ultrathin MoS_2 nanosheets with thickness of approximately 4 nm were clearly observed in a single nanotube (Fig. 2b). Such hierarchical nanostructure can be further observed by TEM investigation. MoS_2 nanotubes clearly exhibited a hollow structure. The surface of the hollow tube is twined by many ultrathin nanosheets. The MoS_2 hollow nanotubes were analyzed by EDS to determine the elementary composition of the samples. The element compositions of the samples contained Cu, Mo, and S. The atomic ratio of S and Mo was calculated to be approximately 2.01, which was equal to the theoretical value of MoS_2. Further investigation on the nanotube structure by HRTEM (Fig. 2e) revealed that the interlayer spacing of MoS_2 was about 0.62 nm, consistent with the (002) plane lattice parameter of hexagonal-phase MoS_2. The HRTEM image of the lattice fringe shown in Fig. 2e indicated that the MoS_2 hollow nanotubes were well crystallized.

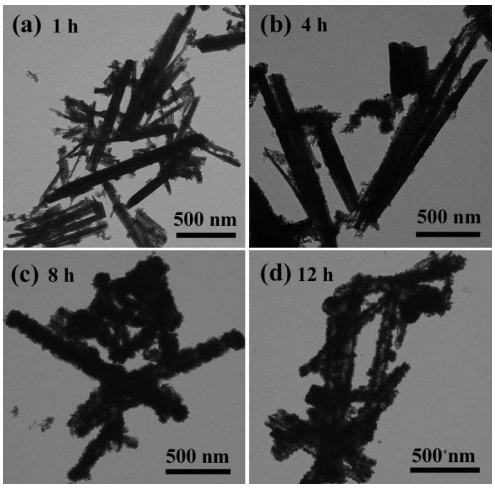

Fig. 3 Typical TEM images of the prepared MoS_2 at different stages: (a) 1 h, (b) 4 h, (c) 8 h, and (c) 12 h, respectively.

More relevant experiments and characterizations were carried out to reveal the growth mechanism of the hierarchical hollow MoS_2 nanotubes. Reaction time plays an important role in the formation of the hierarchical hollow MoS_2 nanotubes. In a typical procedure, the reaction was stopped at different times (1, 4, 8, and 12 h) and the products were detected by XRD and TEM. As shown in Fig. 3a, only solid rods with smooth surface can be obtained when the reaction time was 1 h. The XRD pattern showed that the solid rods were $MnMoO_4$ (JCPDS No. 74-0297) (Fig. 4a). It is demonstrated that the MoO_4^{2-} and Mn^{2+} in the raw reagent formed $MnMoO_4$ in the initial reaction stage. The product after reaction for 4 h was composed of some membrane structure on the smooth surface of the solid rods (Fig. 3b). The intensity of the diffraction peaks of the $MnMoO_4$ became weak and new diffraction peaks of $MnCO_3$ appeared (Fig. 4b). The surface of the rods exhibited more membrane structure (Fig. 3c) and the rod vanished gradually (Fig. 3d) as the reaction time was extended. The diffraction peaks of the $MnMoO_4$ disappeared and the peaks of $MnCO_3$ and MoS_2 appeared after 8 h (Fig. 4c). The $MnMoO_4$ nanorods disappeared gradually as the reaction process. Hollow nanotubes of MoS_2 can be formed in this process. Only some $MnCO_3$ particles dispersed or adhered in the hollow tubes. There are no big differences on the morphology and composition of products (Fig. 4d) at 12 h or 16 h. The reason for the reaction time set at 16 h is that the reaction more fully and the yield is slightly higher than 12 h. In the final products (16 h), some MoS_2 hollow nanotube could be observed indeed before acid washing.

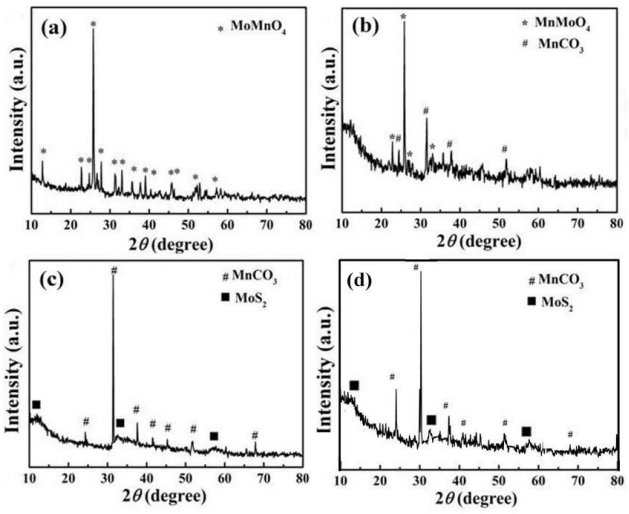

Fig. 4 XRD patterns of the prepared MoS_2 at different stages without any post-treatment: (a) 1 h, (b) 4 h and (c) 8 h, and (d) 16 h, respectively.

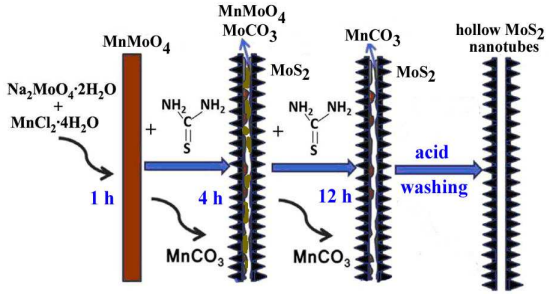

Fig. 5 Illustration of the growth mechanism of the hierarchical hollow MoS_2 nanotubes.

The growth process of hierarchical hollow MoS_2 nanotubes could be elucidated by contrast experiments. First, the Na_2MoO_4 reacted with $MnCl_2$ and formed $MnMoO_4$ nanorods in the initial reaction stage. The $(NH_2)_2CS$ as sulfur source reacted with the $MnMoO_4$ nanorods. MoS_2 nanosheet formed on the surface of $MnMoO_4$ nanorods and the $MnMoO_4$ nanorod as self-sacrificed template disappeared gradually in this reaction process. Finally, hierarchical hollow MoS_2 nanotubes could be formed after washing with HCl acid. A schematic of the formation process for hierarchical hollow MoS_2 nanotubes is shown in Fig. 5.

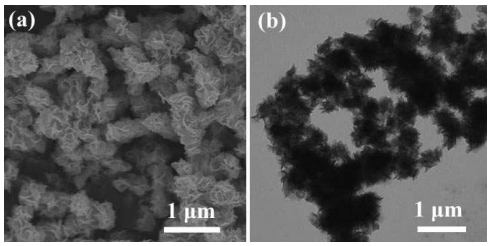

Fig. 6 (a) SEM and (b) TEM images of the MoS_2 nanoflowers.

The effect of solvent on the morphologies of the products was also investigated. The morphology of the MoS_2 sample prepared by the same hydrothermal route with the addition of 10 ml of deionized water and 30 ml absolute ethanol is shown in Fig. 6. Nanoflowers with diameter of approximately 400-500 nm were obtained without nanotubes. Only nanorods or nanosheets could be obtained when using deionized water or ethanol as solvent, respectively. The exact mechanism for the influence of MoS_2 morphology remains unclear at this moment. However, comparing the morphology changes of MoS_2, the proportion of water and ethanol has plays a key role on the formation of MoS_2 nanostructre. In the presence of ethanol in the solvent, nanosheets with thin thickness could easily be formed. The presence of water is beneficial to form the rod structure. Adjusting of the proportion of water and ethanol could leas to different MoS_2 morphologies.

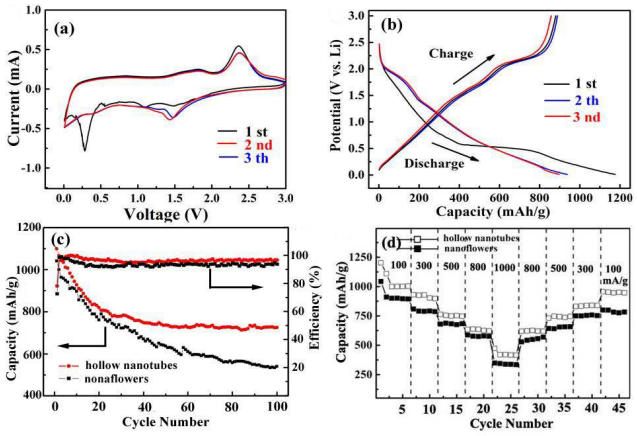

Fig. 7 (a) CV curves of the MoS_2 nanotube electrode in the voltage range of 0.01-3.0 V at 0.1 mV s^{-1}. (b) Discharge/charge curves of the MoS_2 nanotube electrode at 100 mA g^{-1}. (c) Cycling performance and Coulombic efficiency of the MoS_2 nanotubes and MoS_2 nanoflowers at 100 mA g^{-1}. (d) Rate capability of the MoS_2 nanotubes at different current densities.

Electrochemical properties of MoS_2 electrode were investigated by CV and discharge/charge experiments. Fig. 7a shows the CV curves of the hollow MoS_2 nanotube electrode at a scan rate of 0.1 mV s^{-1} in the potential window of 0.01-3.0 V for the first three cycles. During the first cycle, the sharp reduction peak at 0.37 V is attributed to the conversion reduction of the lithium intercalates (Li_xMoS_2) to form metallic Mo and Li_2S.[7,12,32] The small peak at 1.15 V corresponds to the phase transition from trigonal prismatic to octahedral resulting from the intercalation of Li ions.[16,19] In the anodic scan, oxidation at 1.8 V can be attributed to the partial oxidation of Mo to MoS_2, and the following distinct peak located at 2.37 V is associated with the oxidation of Li_2S into S.[7,33] After the first cycle, the electrode was mainly composed of Mo and S instead of the initial MoS_2. Accordingly, in the following cycles, the reduction peak at ~1.5 V indicates the lithiation process of S to form Li_2S,[11,34] and the peak at ~0.37 V corresponds to the disappearance of conversion reaction. Moreover, during the anodic curves in the 2nd and 3rd cycles, the intensity of the peak associated with the oxidation of the Li_2S into S did not exhibit change with cycling, suggesting that equal Li_2S decomposes, significantly contributiing to the stability of the cycling performance.

Fig. 7b shows the first three discharge/charge curves of the hierarchical hollow MoS_2 nanotubes at a current density of 100 mA g^{-1}. An obviously potential plateau at ~0.5 V was observed in the first discharge process. The plateau at 0.5 V could be attributed to a conversion reaction process and formed Mo and Li_2S.[35,36] In the second and third discharge/charge, the MoS_2 electrode displayed two potential plateaus at about 2.0 and 1.8 V and the potential plateau at 0.5 V in the first discharge/charge disappeared. In the charge process, the MoS_2 displayed an inconspicuous potential plateaus at 2.4 V, which is associated with the delithiation of Li_2S to form S. The discharge/charge processes were consistent with the CV curves. The initial discharge and charge capacities of the hierarchical hollow MoS_2 nanotubes were 1197 and 896 mAh g^{-1}. Such a high initial lithium storage capacity may be associated with the unique hierarchical structure of the MoS_2 nanotubes. The irreversible capacity loss was about 21.3%, smaller than that of MoS_2 nanospheres.[37] Fig. 7c shows the cycling performance of MoS_2 nanotubes and nanoflowers at a current density of 100 mA g^{-1}. A reversible capacity as high as 727 mAh g^{-1} can still be retained by the MoS_2 nanotube electrode after 100 cycles. The first initial Coulombic efficiency was 76.2%. The discharge and charge capacities in the second cycle are 942 and 883 mAh g^{-1}, giving rise to a Coulombic efficiency of 93.7% and this value further increase to 95.5% in the third cycle. The Coulombic efficiency became stable and larger than 95% after the third cycle. In contrast, the flower-like MoS_2 delivered a capacity of 520 mAh g^{-1} whereas the commercial MoS_2 can only exhibits a much lower capacity of 300 mAh g^{-1}. The initial capacity fading mainly attributed to the decomposition of the electrolyte and the formation of the solid electrolyte inter-phase (SEI) layer at the surface of the MoS_2 electrode materials. Second, some of the Li^+ ions are trapped in the disordered structure after initial cycles. Furthermore, volume change during the discharge/charge cycles can result in structural instability and capacity decreasing. All of these reason will lead to capacity fading. In addition to the cycling stability, the high-rate capability is also of great importance especially for high-power applications. Given their unique structure, these MoS_2 nanotube materials exhibit excellent rate capability in varying current densities. Even when cycled at a high rate of 1000 mA g^{-1}, discharge capacities of 480 mAh g^{-1} can still be maintained, as shown in Fig. 7d. After deep discharged at 1000 mA g^{-1}, a stable capacity of 900 mAh g^{-1} can be restored when the current density is reduced back to 100 mA g^{-1}. Among the two samples (MoS_2 nanotubes and nanoflowers), the MoS_2 nanotubes exhibited significantly higher capacity, and better cycling stability and rate capability, which may be attributed to their unique structural features. In detail, the formed hollow and hierarchical structures endow the material with obvious increment of reactive sites and

enhance the electrolyte/electrode contact area, as well as shorten the Li^+ ions diffusion length. N_2 adsorption/desorption isotherms (Fig. S1, EIS†) are further used to investigate the effects of the specific surface area and pore structure on cycling performance. The hierarchical MoS_2 hollow nanotubes have much higher BET specific surface area (21.3 m^2g^{-1}) than the MoS_2 nanoflowers (10.8 m^2g^{-1}). Furthermore, the presence of hollow tubes provides effective buffering for volume effect during Li^+ insertion/extraction. Therefore, the hierarchical MoS_2 hollow nanotubes reasonably show better cycling stability and rate capability than the MoS_2 nanoflowers and particles. The morphology changes after cycling of MoS_2 hollow nanotubes and nanoflowers have been provided (Fig. S2, EIS†). It was found that hollow nanotube structure of MoS_2 also could be observed after 100 cycles. But nanoflower pulverization was very serious, and flower-like structure cannot be observed nearly.

These solid MoS_2 particles in a size of 200-700 nm prepared by the similar procedure only displayed 410 mAh g^{-1} after 80 cycles.[38] In order to further compare the electrochemical performance of the typical pure MoS_2 materials, some relevant information are summarized (Table S1, ESI†).

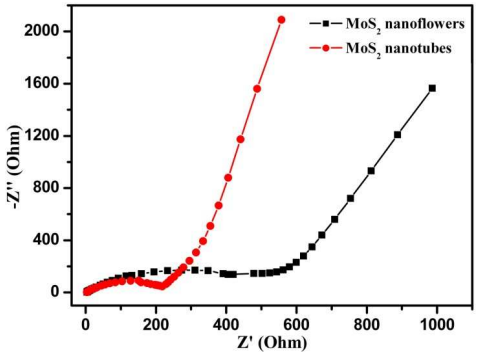

Fig. 8 Nyquist plots of the MoS_2 nanotube and nanoflower electrode at open-circuit voltage.

EIS was detected to further study the electrochemical performance of MoS_2 electrode materials. Fig. 8 shows the Nyquist plots of the MoS_2 nanoflower and nanotube electrodes, respectively. The depressed semicircles at high frequency are related to the charge transfer process and the numerical diameter of the semicircle on the Z_{re} axis is equal to the charge transfer resistance (R_{ct}).[39] The Warburg impedance is associated with Li^+ diffusion in the electrode, corresponding to the inclined line at low frequency. The R_{ct} value is 230 Ω for the MoS_2 hollow nanotubes, much lower than that of MoS_2 nanoflower electrodes (550 Ω), indicating that MoS_2 hollow nanotubes have high electronic and ionic conductivites.[40,41] This result further confirmed that hollow structure and hierarchical surface contributed to significantly improve the electrolyte/electrode contact area, shorten the Li^+ diffusion length, and alleviate the volume effect during the discharge-charge cycles, which are very important to improve the electrochemical performance of the batteries.

4. Conclusions

This study presented a facile method for the synthesis of hierarchical hollow MoS_2 nanotubes. The MoS_2 nanotubes showed excellent cycle stability with high specific capacity and outstanding rate capability when used as a material for anode in LIBs. At a current density of 100 mA g^{-1}, the MoS_2 nanotubes exhibited stable capacity of 727 mA g^{-1} after 100 cycles. The improvement in the electrochemical performance of the material can be attributed to their unique structure, which can facilitate Li^+ ion diffusion and electrolyte permeated internal of electrode. These results demonstrated that hierarchical hollow MoS_2 nanotubes are promising anode electrodes for LIBs.

Acknowledgements

This work was supported by National Nature Science Foundation of China (Grant No. 21301102) and Scientific Research Foundation of Shandong Province Outstanding Young Scientist Award (Grant No. BS2013CL023).

Notes and references

[a] *School of Chemistry and Pharmaceutical Engineering, Qilu University of Technology, Jinan 250353, China. Fax: +86 531 89631070; Tel: +86 531 89631075; E-mail:ligd@qlu.edu.cn*
[b] *Hongyunhonghe Technology Center, Tobacco Yunnan Industrial Co., Ltd, Kunming 650202, China.Fax: +86 871 65869555; Tel: +86 871 65869555; E-mail: wangm_chemistry@sina.com*
† Electronic supplementary information (EIS) available.

1 M. Armand and J. M. Tarascon, *Nature*, 2009, **42**, 713.
2 J. B. Goodenough and Y. Kim, *Chem. Mater.*, 2010, **22**, 587.
3 K. S. Kang, Y. S. Meng, J. Breger, C. P. Grey and G. Ceder, *Science*, 2006, **311**, 977.
4 M. Sathish, T. Tomai, I. Honma, J. Power Source, 2012, 217, 85.
5 X. Z. Zheng, Y. F. Li, Y. X. Xu, Z. S. Hong and M. D. Wei, *CrystEngComm*, 2012, **14**, 2112.
6 Y. Wang, M. Wu, Z. Jiao and J. Y. Lee, *Chem. Mater.*, 2009, **21**, 3210.
7 J. Xiao, X. Wang, X. Q. Yang, S. Xun, G. Liu, P. K. Koech, J. Liu and J. P. Lemmon, *Adv. Funct. Mater.*, 2011, **21**, 2840.
8 B. Luo, B. Fang, Y. Wang, J. Zhou, H. Song and L. Zhi, *Energy Environ. Sci.*, 2012, **5**, 5226.
9 H. Liu, D. Su, G. Wang and S. Z. Qiao, *J. Mater. Chem.*, 2012, **22**, 17437.
10 S. Liang, J. Zhou, J. Liu, A. Pan, Y. Tang, T. Chen and G. Fang, *CrystEngComm*, 2013, **15**, 4998.
11 L. Zhang and X. W. Lou, *Chem. Eur. J.*, 2014, **20**, 5219.
12 L. Yang, S. Wang, J. Mao, J. Deng, Q. Gao, Y. Tang and O. G. Schmidt, *Adv. Mater.*, 2013, **25**, 1180.
13 K. Zhang, H. Kim, X. Shi, J. Lee, J. Choi, M. Song and J. H. Park, *Inorg. Chem.*, 2013, **52**, 9807.
14 C. F. Zhang, Z. Y. Wang, Z. P. Guo and X. W. Lou, *ACS Appl. Mater. Interfaces*, 2012, **4**, 3765.
15 S. K. Park, S. H. Yu, S. Woo, J. Ha, J. Shin, Y. E. Sung and Y. Piao, *CrystEngComm*, 2012, **14**, 8323.
16 S. Ding, D. Zhang, J. S. Chen and X. W. Lou, *Nanoscale*, 2012, **4**, 95.
17 C. F. Zhang, H. B. Wu, Z. P. Guo and X. W. Lou, *Electrochem. Commun.*, 2012, **20**, 7.
18 S. K. Park, S. H. Yu, S. Woo, B. Quan, D. C. Lee, M. K. Kim, Y. E. Sung and Y. Piao, *Dalton Trans.*, 2013, **42**, 2399.
19 S. J. Ding, J. S. Chen and X. W. Lou, *Chem. Eur. J.*, 2011, **17**, 13142.
20 S. K. Das, R. Mallavajula, N. Jayaprakash and L. A. Archer, *J. Mater. Chem.*, 2012, **22**, 12988.
21 K. Bindumadhavan, S. K. Srivastava and S. Mahanty, *Chem. Commun.*, 2013, **49**, 1823.
22 J. Z. Wang, L. Lu, M. Lotya, J. N. Coleman, S. L. Chou, H. K. Liu, A. I. Minett and J. Chen, *Adv. Energy Mater.*, 2013, **3**, 798.
23 X. Zhou, L. J. Wan and Y. G. Guo, *Nanoscale*, 2012, **4**, 5868.

24 K. Chang, W. Chen, L. Ma, H. Li, H. Li, F. Huang, Z. Xu, Q. Zhang and J. Y. Lee, *J. Mater. Chem.*, 2011, **21**, 6251.
25 K. Chang and W. X. Chen, *ACS Nano*, 2011, **5**, 4720.
26 X. Zhou, L. J. Wan and Y. G. Guo, *Chem. Commun.*, 2013, **49**, 1838.
27 V. H. Pham, K. H. Kim, D. W. Jung, K. Singh, E. S. Oh and J. S. Chung, *J. Power Source*, 2013, **244**, 280.
28 K. Chang and W. X. Chen, *J. Mater. Chem.*, 2011, **21**, 17175.
29 H. Yu, C. Ma, B. Ge, Y. Chen, Z. Xu, C. Zhu, C. Li, Q. Ouyang, P. Gao, J. Li, C. Sun, L. Qi, Y. Wang and F. Li, *Chem. Eur. J.*, 2013, **19**, 5818.
30 W. W. Li, X. F. Wang, B. Liu, S. Luo, Z. Liu, X. J. Hou, Q. Y. Xiang, D. Chen and G. Z. Shen, *Chem. Eur. J.*, 2013, **19**, 8650.
31 W. W. Li, X. F. Wang, B. Liu, J. Xu, B. Liang, T. Luo, S. Luo, D. Chen and G. Z. Shen, *Nanoscale*, 2013, **5**, 10291.
32 X. Xu, Z. Y. Fan, X. Y. Yu, S. J. Ding, D. Yu and X. W. Lou, *Adv. Energy Mater.*, 2014, DOI: 10.1002/aenm.20140902.
33 Y. Miki, D. Nakazato, H. Ikuta, T. Uchida and M. Wakihara, *J. Power Source*, 1995, **54**, 508.
34 X. P. Fang, X. W. Guo, Y. Mao, C. X. Hua, L. Y. Shen, Y. S. Hu, Z. X. Wang, F. Wu and L. Q. Chen, *Chem. Asian J.*, 2012, **7**, 1013.
35 S. E. Cheon, K. S. Ko, J. H. Cho, S. W. Kim and H. T. Kim, *J. Electrochem. Soc.*, 2003, **150**, A800.
36 J. L. Wang, J. Yang, C. R. Wan, K. Du, J. Y. Xie and N. X. Xu, *Adv. Mater.*, 2003, **13**, 487
37 J. Zhao, F. Q. Wang, P. P. Su, M. G. Li, J. Chen, Q. H. Yang and C. Li, *J. Mater. Chem.*, 2012, **22**, 13328.
38 X. Chen, L. Qie, L. Zhang, W. Zhang and Y. Huang, *J. Alloys Compd.*, 2013, **559**, 5.
39 A. Y. Shenouda and H. K. Liu, *J. Alloys Compd.*, 2009, **477**, 498.
40 B. Jin, E. M. Jin, K. H. Park and H. B. Gu, *Electrochem. Commun.*, 2008, **10**, 1537.
41 A. Y. Shenouda and H. K. Liu, *J. Electrochem. Soc.*, 2010, **157**, A1183.

Novel hierarchical hollow MoS_2 nanotubes have been fabricated, which exhibited excellent electrochemical performance as an anode material for lithium-ion batteries.